Stomatal optimisation based on xylem hydraulics (SOX) improves land surface model simulation of vegetation responses to climate

New Phytologist

Stomatal optimisation based on xylem hydraulics (SOX) improves land surface model simulation of vegetation responses to climate

Journal:	*New Phytologist*
Manuscript ID	NPH-MS-2019-31667.R1
Manuscript Type:	MS - Regular Manuscript
Date Submitted by the Author:	n/a
Key Words:	climate change, drought, eddy covariance, land-surface models, stomata optimization models, xylem hydraulics

Complete List of Authors:

Eller, Cleiton; University of Exeter, Department of geography
Rowland, Lucy; University of Exeter, Department of Geography; University of Exeter, Department of Geography
Mencuccini, Maurizio; CREAF, Universidad Autonoma de Barcelona, c/o, CREAF; Pg. Lluís Companys 23, ICREA
Rosas, Teresa; Universitat Autonoma de Barcelona Centre de Recerca Ecologica i Aplicacions Forestals, Biologia Animal, Vegetal i Ecologia
Medlyn, Belinda; Western Sydney University Hawkesbury Institute for the Environment, Ecosystem Function and Integration
Williams, Karina; Met Office, Hadley Centre
Harper, Anna; University of Exeter, College of Engineering, Mathematics and Physical Sciences
Wagner, Yael; Weizmann Institute of Science, Department of Plant and Environmental Sciences
Klein, Tamir; Weizmann Institute of Science, Department of Plant and Environmental Sciences
Teodoro, Grazielle; University of Campinas, Plant Biology
Oliveira, Rafael; University of Campinas, Plant Biology
Matos, Ilaíne ; Universidade do Estado do Rio de Janeiro, Instituto de Biologia Roberto Alcântara Gomes
Rosado, Bruno; Universidade do Estado do Rio de Janeiro, Ecologia;
Fuchs, Kathrin; ETH Zurich Department of Environmental Systems Science, Department of Environmental Systems Science
Wohlfahrt, Georg; University of Innsbruck, Ecosystem Research & Landscape Ecology
Montagnani, Leonardo; Free University of Bolzano Faculty of Science and Technology, Faculty of Science and Technology
Meir, Patrick; Australian National University, Research School of Biology; University of Edinburgh, School of Geosciences
Sitch, Stephen; University of Exeter, College of Life and Environmental Sciences ; University of Leeds, School of Geography
Cox, Peter; University of Exeter, School of Engineering, Mathematics and Physical Sciences

Stomatal optimisation based on xylem hydraulics (SOX) improves land surface model simulation of vegetation responses to climate

Eller CB[1,2], Rowland L[1], Mencuccini M[3,4], Rosas T[3,4], Williams K[5], Harper A[6], Medlyn BE[7], Wagner Y[8], Klein T[8], Teodoro GS[9], Oliveira RS[2], Matos IS[10], Rosado BHP[10], Fuchs K[11], Wohlfahrt G[12], Montagnani L[13], Meir P[14,15], Sitch S[1], Cox PM[6]

[1]College of Life and Environmental Sciences, University of Exeter, Exeter, EX4 4QF, UK; [2]Department of Plant Biology, University of Campinas, Campinas, 13083-862, Brazil; [3]CREAF, Barcelona, Spain. [4]ICREA, Barcelona, Spain; [5]Met Office Hadley Centre, Fitzroy Road, Exeter, EX1 3PB, UK; [6]College of Engineering, Mathematics and Physical Sciences, University of Exeter, Exeter, EX4 4QF, UK; [7]Hawkesbury Institute for the Environment, Western Sydney University, Locked Bag 1797, Penrith NSW 2751 Australia; [8]Department of Plant & Environmental Sciences, Weizmann Institute of Science, 76100 Rehovot, Israel; [9]Institute of Biological Sciences, Federal University of Pará, Belém, 66075-110, Brazil; [10]Department of Ecology - IBRAG, Rio de Janeiro State University (UERJ), 20550-013, Brazil; [11]Department of Environmental Systems Science, ETH Zurich, Universitätstrasse 2,8092 Zurich, Switzerland; [12]Department of Ecology, University of Innsbruck, Innsbruck, 6020, Austria; [13]Forest Services, Autonomous Province of Bolzano, Via Brennero 6, 39100 Bolzano, Italy; [14]Research School of Biology, The Australian National University, Acton ACT 2601, Australia; [15]School of Geosciences, University of Edinburgh, Edinburgh EH93FF, UK

Author for correspondence:

Cleiton B. Eller

Email: c.breder-eller@exeter.ac.uk

Main text word count	6420	No. figures	6 (all color)
Summary	190	No. of Supporting Information files	1
Introduction	1174		
Material and Methods	1948		
Results	1441		
Discussion	1857		
Acknowledgments	118		
No. Tables	3		

Summary

- Land surface models (LSMs) typically use empirical functions to represent vegetation responses to soil drought. These functions largely neglect recent advances in plant ecophysiology that link xylem hydraulic functioning with stomatal responses to climate.
- We developed an analytical stomatal optimisation model based on xylem hydraulics (SOX) to predict plant responses to drought. Coupling SOX to the Joint UK Land Environment Simulator (JULES) LSM, we conducted a global evaluation of SOX against observations.
- SOX simulates leaf stomatal conductance responses to climate for woody plants more accurately and parsimoniously than the existing JULES stomatal conductance model. An ecosystem-level evaluation at 70 eddy flux sites shows that SOX decreases the sensitivity of gross primary productivity (GPP) to soil moisture, which improves the model agreement with observations and increases the predicted annual GPP by 30%. SOX decreases JULES root mean squared error in GPP by up to 45 % in evergreen tropical forests, and can simulate realistic patterns of canopy water potential and soil water dynamics at the studied sites.
- SOX provides a parsimonious way to incorporate recent advances in plant hydraulics and optimality theory into LSMs, and an alternative to empirical stress factors.

Keywords: climate change, drought, eddy covariance, land-surface models, stomatal optimization, xylem hydraulics.

Introduction

Large areas of the globe will be exposed to increased aridity in the near future (Sheffield & Wood, 2008; Duffy *et al.*, 2015; Marengo *et al.*, 2018). As drought events become more intense and frequent, accurately representing vegetation-climate feedbacks in Earth System Models (ESMs) is increasingly important, as these interactions can drastically influence model projections of global climate change (Cox *et al.*, 2000). The current generation of Land Surface Models (LSMs) does not accurately simulate vegetation carbon dynamics during drought (Sitch *et al.*, 2008; Powell *et al.*, 2013; Medlyn *et al.*, 2016; Ukkola *et al.*, 2016; Restrepo-Coupe *et al.*, 2017; Rogers *et al.*, 2017; Eller *et al.*, 2018b), thereby restricting our capability to predict the effect of increased aridity on vegetation distribution and its feedbacks on the global carbon cycle and climate. Many LSMs represent the effects of reduced soil moisture on canopy carbon assimilation (A) using an empirical drought factor commonly referred as β-factor (Cox *et al.*, 1998). The β-factor approach has been shown to overestimate plant responses to seasonal and experimentally induced drought (Ukkola *et al.*, 2016; Restrepo-Coupe *et al.*, 2017; Eller *et al.*, 2018b). The β-factor has a large impact on the modelled global carbon budget, supressing 30-40% of the annual gross primary productivity (GPP) in large areas of arid and semi-arid ecosystems (Trugman *et al.,* 2018). Despite its importance, there is scarce empirical support for the drought functions used in most LSMs (Medlyn *et al.,* 2016). The lack of a theoretical or empirical basis for the β-factor implies an urgent need for new modelling approaches to replace this important component of LSMs so as to improve our capacity to predict vegetation-climate interactions.

Stomatal responses of plants to soil drought involve complex chemical signalling and hydrodynamic processes in leaf cells, some of which have not been entirely elucidated (Buckley, 2017; 2019; Qu *et al.,* 2019). Stomatal optimization models are a useful approach to model

stomatal behaviour that circumvents the need to explicitly represent the physiological processes involved in stomatal regulation. Optimization models employ a 'goal-oriented' approach, assuming that plant stomata behaviour has been selected through plant evolutionary history to maximize a given objective function (Cowan, 2002; Dewar *et al.*, 2009; Prentice *et al.* 2014; Buckley, 2017). The traditional approach to model optimal stomatal behaviour is derived from the seminal work of Cowan & Farquhar (1977). This approach proposes that optimal stomatal behaviour maximizes A minus the carbon cost of water lost (λE) over a given time interval, where E is transpiration and λ is the lagrange multiplier that represents the carbon cost of a unit of water lost. This model, hereafter labelled CF, after Cowan & Farquhar, is capable of simulating many patterns of stomatal responses to climate over short time scales (Farquhar *et al.*, 1980; Berninger & Hari, 1993), and has provided the theoretical basis for several widely used semi-empirical stomatal models (Jacobs, 1994; Leuning, 1995; Medlyn *et al.*, 2011). However, CF predicts that stomatal conductance (g_s) increases in response to elevated CO_2 when A is Rubisco-limited, which contradicts most observations (Mott, 1988; Medlyn *et al.*, 2001). Other limitations are related to the λ, as the CF hypothesis does not link λ to measurable plant traits or environmental quantities (Buckley, 2017), and assumes λ is constant over the period of reference (Cowan & Farquhar, 1977), which makes the original CF unable to predict long-term g_s decline in response to soil moisture depletion.

Since the original CF work many attempts have been made to incorporate the effects of declining soil moisture in the CF stomatal optimization framework (Cowan, 1986; Mäkelä *et al.*, 1996; Williams *et al.*, 1996; Manzoni *et al.*, 2013). Some of these attempts, such as the Soil-Plant-Atmosphere (SPA) model of Williams *et al.* (1996), employ principles of plant hydraulics to constrain stomatal optimization and have been successfully incorporated into LSMs (Bonan *et al.*,

2014). The numerical approach used by SPA employs a hydraulic threshold to set a lower water potential limit (Ψ_{min}) for g_s, which simulates a strict isohydric stomatal regulation (Fisher *et al.*, 2006). Despite using plant hydraulics SPA still relies on a water-use efficiency optimization similar to CF to model stomatal behaviour when $\Psi > \Psi_{min}$ (Williams *et al.,* 1996; Bonan *et al.,* 2014).

Alternative routes to model plant optimal stomatal behaviour have been proposed recently (see Mencuccini *et al.*, 2019a for a review). These approaches circumvent the CF limitations by assuming plant optimal stomatal behaviour minimizes the instantaneous fitness costs associated with low Ψ. These new optimization models use widely available plant hydraulic traits (Kattge *et al.*, 2011; Choat *et al.*, 2012) to simulate g_s responses to environmental conditions, producing a realistic g_s decline in response to elevated atmospheric CO_2 and soil drought (Sperry *et al.*, 2017; Eller *et al.*, 2018b; Venturas *et al.*, 2018; Wang *et al.,* 2019). This approach predicts a tight coordination between stomatal and xylem functioning which is widely corroborated by observations (Hubbard *et al.*, 2001; Meinzer *et al.*, 2009; Klein, 2014). Another advantage of this approach is its capacity to simulate a diversity of contrasting stomatal behaviours, from iso to anisohydric (Martinez-Vilalta *et al.,* 2014; Klein, 2014).

Sperry *et al.* (2017) proposes a model that assumes that, as xylem hydraulic conductance declines, the increased risk of hydraulic failure is the main fitness cost associated with low Ψ. Eller *et al*. (2018b) adapted the Sperry *et al.* (2017) model into the stomatal optimization model based on xylem hydraulics (SOX), which principally differs from the Sperry *et al.* (2017) model by using a different optimization target. The SOX optimization target is based on the PGEN model (Friend, 1995), which assumes stomata optimize plant dry matter production, represented by the product of photosynthesis and a linear function of Ψ. The SOX model in Eller *et al.* (2018b) uses a

numerical routine to find the optimum g_s. However, the PGEN optimization target can also be found analytically (Friend & Cox, 1995; Dewar *et al.*, 2018). A parsimonious analytical formulation for SOX would facilitate its incorporation into existing LSMs and provide a practical alternative to the β-function for modelling stomatal responses to drought at global scales.

In this study we develop an analytical approximation for the numerical SOX model presented in Eller *et al.* (2018b). We then create a new configuration for the Joint UK Land Environment Simulator (JULES; Best *et al.,* 2011; Clark *et al.,* 2011) that uses SOX to compute vegetation g_s from environmental and plant hydraulic data. Using a global dataset of xylem hydraulic traits, together with an extensive leaf gas-exchange and eddy covariance dataset, we calibrate the SOX parameters and compare the JULES-SOX performance to the default JULES using the β-function, across all major global biomes. Our goals in this paper are twofold: 1- To test SOX agreement with global observations of g_s to assess the generality of the underlying hypothesis in SOX, that is, that plant stomata evolved to balance carbon assimilation with the loss of hydraulic conductance; and 2 – To evaluate the effect of SOX on JULES ecosystem-scale predictions of carbon and water fluxes, and their agreement with observations.

Materials and Methods

Analytical SOX description

The SOX central hypothesis can be summarised as '*stomatal conductance (g_s) is such as to maximise the product of leaf photosynthesis and xylem hydraulic conductance'* and given by:

$$A(c_i(g_s))\,K(\Psi_m(g_s)) \qquad (Eqn\ 1)$$

where A is leaf net CO_2 assimilation (mol CO_2 m^{-2} s^{-1}), which is a function of leaf internal CO_2 partial pressure (c_i; Pa), which is itself a function of stomatal conductance to CO_2 (g_s; mol m^{-2} s^{-1}). The K is the normalised (0 to 1) xylem hydraulic conductance computed as:

$$K(\Psi) = \frac{1}{\left[1 + \left(\Psi/\Psi_{50}\right)^{a}\right]} \quad (Eqn\ 2)$$

where Ψ_{50} is Ψ when K = 0.5 and the parameter a gives the shape of the curve, with a higher a producing a steeper response to Ψ. We use the mean (Ψ_m; MPa) of the canopy water potential at the predawn (Ψ_{pd}; MPa) and the canopy water potential (Ψ_c; MPa) to compute K with equation 2 to account for the gradual decline in Ψ along the soil to canopy hydraulic pathway (see details in Notes S1). The g_s value that maximises equation 1 is found at:

$$\frac{\partial AK}{\partial g_s} = 0 \quad (Eqn\ 3)$$

The g_s value that satisfies equation 3 was found numerically in Eller *et al.* (2018b), but a computationally efficient analytical solution is preferable for application in Dynamic Global Vegetation Models (DGVMs) and ESMs. We developed an analytical approximation for the optimal SOX g_s using the partial derivatives of A with respect to c_i and K with respect to Ψ_m. All steps of the model derivation are described in Notes S1. The resulting SOX equation for the optimal g_s is:

$$g_s = 0.5\frac{\partial A}{\partial c_i}\left(\sqrt{\frac{4\xi}{\partial A/\partial c_i} + 1} - 1\right) \quad (Eqn\ 4)$$

The benefit of stomatal opening is represented here by the sensitivity of leaf photosynthesis to the internal CO_2 concentration ($\partial A/\partial c_i$). By constrast, the parameter ξ represents the cost of stomatal opening in terms of loss of xylem conductivity under low Ψ_{pd} and/or higher leaf-to-air vapour pressure (D; mol mol^{-1}):

$$\xi = \frac{2}{1/K\ \partial K/\partial \Psi_m\ r_p 1.6D} \quad (Eqn\ 5)$$

Low ξ indicates high hydraulic costs occurring during drought (i.e. lower Ψ_{pd} and higher D, Fig. S1). SOX simulates dynamic changes on the plant hydraulic resistance (r_p) computing r_p as a function of Ψ_{pd} and the plant minimum hydraulic resistance (r_{pmin}, m^2 s MPa mol^{-1} H_2O):

$$r_p = \frac{r_{p,min}}{K(\Psi_{pd})} \quad (Eqn\ 6)$$

Solving SOX main equations (Eqn 4-5) requires computing the partial derivatives of A and K, $\partial A/\partial c_i$ and $\partial K/\partial \Psi_m$, respectively. These derivatives were estimated numerically in this study as described in Notes S2.

We evaluated SOX as a stand-alone leaf-level model, and coupled to JULES, hereafter JULES-SOX. The leaf-level model was evaluated against leaf gas exchange data as an 'assumption centred' (*sensu* Medlyn *et al.*, 2015) test of the hypothesis underlying SOX. The JULES-SOX was then evaluated against ecosystem-level eddy flux data, which constituted the first practical test of the utility of SOX for LSMs.

JULES β-function description

The JULES model (Best *et al.*, 2011; Clark *et al.*, 2011) uses the Collatz *et al.* (1991, 1992) photosynthesis model for C_3 and C_4 plants (Notes S3) to produce unstressed rates of A based on the co-limitation of light, Rubisco carboxylation capacity, and the transport of photoassimilates (for C_3 plants) and PEPcarboxylase limitation (for C_4 plants). The effect of soil moisture in A in the default JULES is given by multiplying A by the β factor, computed using the β-function from Cox *et al* (1998):

$$\beta = \begin{cases} 1 \ for\ \theta > \theta_c \\ \dfrac{\theta - \theta_w}{\theta_c - \theta_w} \ for\ \theta_w < \theta \leq \theta_c \\ 0\ for\ \theta \leq \theta_w \end{cases} \quad (Eqn\ 7)$$

where θ is the mean soil moisture in the root zone ($m^3\ m^{-3}$), and θ_c and θ_w, are the critical and wilting points, which are defined by Cox *et al.* (1998) as the θ when soil Ψ is -0.033 and -1.5 MPa, respectively. The default JULES formulation employs the Jacobs (1994) equation to predict c_i from D, c_a and the CO_2 compensation point, Γ (Pa):

$$c_i = f_0\left(1 - \frac{D}{D_{crit}}\right)(c_a - \Gamma) + \Gamma \qquad (Eqn\ 8)$$

where f_0 and D_{crit} are empirical parameters (Jacobs, 1994; Cox *et al.,* 1998).

The JULES-SOX configuration replaces equations 7-8, computing g_s from environmental data and plant hydraulic inputs with equations 4-5. To compute A from the g_s predicted by equation 4, we solved the limiting photosynthetic rates from the Collatz *et al.* (1991; 1992) model as functions of c_a and g_s, as described in Notes S3.

Leaf-level SOX evaluation

We used a global compilation of leaf gas exchange data to evaluate the SOX capacity to reproduce leaf stomatal responses of a wide range of woody plants. This dataset contains observations compiled by Lin *et al.* (2015), complemented with other published and unpublished data (see Table S1 and Fig. S2 for additional information). In total, there are 3597 measurements of g_s and Ψ_{pd} together with environmental variables used for driving the model, that is: incident photosynthetic active radiation (I_{par}), air temperature (T_a), c_a and D. This data comes from 30 woody plant species collected in 15 sites around the world (Fig. S2b). The Ψ_{pd} was measured on the same day as g_s, and the environmental data was measured simultaneously with g_s. The dataset included field and greenhouse observations, with environmental conditions varying from well-watered to extreme drought (Ψ_{pd} = -7 MPa). These observations were grouped into the global Plant Functional Type (PFT) categories from Harper et al (2016) (Table 1). Harper *et al.* (2016) divides Angiosperms tree species into Broadleaved Evergreen Tropical Trees (BET-Tr), Broadleaved

Evergreen Temperate Trees (BET-Te) and Broadleaved Deciduous Trees (BDT), while Gymnosperms tree species are divided into Needle-leaved Evergreen Trees (NET) and Needle-leaved Deciduous Trees (NDT). Shrub species were divided into Evergreen Shrubs (ESh) and Deciduous Shrubs (DSh), and two grass PFTs defined by their photosynthetic pathway (C_3 and C_4). The grass PFTs and the NDT were excluded from the leaf-level evaluation because no stomatal conductance data were available for these PFTs in the dataset used in this study.

The plant hydraulic parameters used in SOX (i.e. Ψ_{50}, a, and r_{pmin}) were fitted to the g_s data using an algorithm that minimizes the model residual sum of squares within the constraints of the observed Ψ_{50}, a and r_{pmin}. We compiled hydraulic data for each PFT from the literature to constrain the leaf-level model fit. The Ψ_{50} for woody plants was obtained from a version of the Choat *et al.* (2012) dataset updated recently by Mencuccini *et al.* (2019b). The shape parameter a of the xylem vulnerability function (Eqn 2) was estimated from the linear gradient between Ψ_{50} and the Ψ when the plant loses 88% of its maximum hydraulic conductance. The r_{pmin} was estimated from branch-level hydraulic conductivity measurements scaled from branch to whole plant taking into account plant height, Huber value and xylem tapering using the calculations described in Christoffersen *et al.* (2016) and Savage *et al.* (2010) (Notes S4). All the data used for these calculations were obtained from the hydraulic dataset from Mencuccini *et al* (2019b). We note that scaling branch to whole tree r_{pmin} requires several assumptions about tree hydraulic architecture (Notes S4). Therefore, the presented values of r_{pmin} must be considered as a reference useful only to assess if the r_{pmin} input values used in the model are within the same order of magnitude of the observations. The other parameters of the photosynthesis model used in SOX (Notes S3) were set equal to Harper *et al.* (2016).

The model predictive skill was evaluated using the model root mean squared errors (RMSE) and the Nash and Sutcliffe (1970) model efficiency index (NSE). The NSE varies from -∞ to 1, with 1 indicating perfect agreement between model and observations, while NSE < 0 indicates the mean value of the observations is a better predictor than the model. The model parsimony was evaluated using the Akaike Information Criterion (AIC), which penalizes model overparameterization (Bozdogan, 1987). We compared SOX AIC score with the β-function (Eqn 7-8). The parameters f_0 and D_{crit}, (Eqn 8) were fitted to the PFT g_s data, while the θ_c and θ_w were held at their default values (-0.033 and -1.5 MPa, respectively).

The uncertainty in plant hydraulic parameters caused by within PFT hydraulic variability was propagated to the model predictions using bootstrapped 95% confidence intervals. We created the interval based on 1000 model runs with parameters resampled from the hydraulic trait data for each PFT.

Eddy-covariance based JULES-SOX evaluation

We evaluated default JULES and JULES-SOX against daily gross primary productivity (GPP) estimates derived from eddy flux tower data at 62 FLUXNET sites (http://fluxnet.fluxdata.org, Baldocchi *et al.,* 2001) and 8 LBA sites (https://daac.ornl.gov/LBA, Saleska *et al.,* 2013) covering all the major biomes of the world (Fig. S2, Table S2). In 10 of these sites we also had data for surface (5 to 15 cm) soil moisture content, which was used to evaluate the model soil moisture dynamics predictions. We classified the land cover on each site using the International Geosphere-Biosphere Programme (IGBP) classification (Loveland *et al.*, 2000). Each site was classified as one of the following categories according to its prescribed PFT cover (Table S2): cropland (CRO), deciduous broadleaf forests (DBF), deciduous needleleaf forests (DNF), temperate evergreen broadleaf forests (EBF-Te), tropical evergreen broadleaf forests (EBF-Tr), evergreen needleleaf

247 forest (ENF), grassland (GRA), mixed forest (MF), savannah (SAV), shrubland (SHR), and
248 wetlands (WET). We grouped the IGBP categories open and closed shrublands into SHR, as we
249 only had a single closed shrubland site. Similarly, woody savannah was grouped with SAV, as we
250 only had two woody savannah sites. We divided the evergreen broad leaf forests category into
251 EBF-Te and EBF-Tr, as these sites were dominated by distinct PFTs (BET-Te and BET-Tr,
252 respectively).

253 We evaluated JULES-SOX using the SOX hydraulic parameters (i.e. Ψ_{50}, a, and r_{pmin}) that
254 minimized the residual sum of squares between SOX predictions and the eddy flux GPP
255 observations from a subset of the sites used for model evaluation (Fig. S2; Table S2). Each site
256 was used to calibrate the hydraulic parameters for its dominant PFT (i.e. the PFT covering more
257 than 50% of the site area), except for DSh, which was not dominant in any of the available sites.
258 We used a site with DSh cover of 35% (US-SRM) to calibrate the hydraulic parameters of this
259 PFT. The hydraulic parameters of the others PFTs (if any) present on the site were kept constant
260 during the model runs for parameter calibration. Similar to the leaf-level evaluation, the parameter
261 calibration in JULES-SOX was constrained within the range of the observed values of Ψ_{50}, a, and
262 r_{pmin} for all PFTs, except NDT which did not have enough observations to satisfactorily constrain
263 the model parameters. The Ψ_{50} for grasses was obtained from Lens *et al.* (2016) dataset updated
264 with data from Ocheltree *et al.* (2016).

265 *Model setup*

266 The JULES and JULES-SOX configuration used in this study employed the 10-layer canopy
267 scheme with sunlit and shaded leaves in each layer as described in Clark *et al.* (2011). The canopy
268 radiation profile was given by the two-stream approach from Sellers (1985), with the sun-fleck
269 penetration scheme from Mercado *et al.* (2009), and an exponential decrease of photosynthetic

capacity through the canopy (Mercado *et al.*, 2007). All the model runs used in this study were site-level simulations driven with hourly local meteorological data. Vegetation dynamics (Cox, 2001) was turned off and the site PFT coverage by site was prescribed based on the site vegetation description obtained from the site principal investigators (Table S3) or information from the site available on the FLUXNET website (https://fluxnet.fluxdata.org/sites/site-list-and-pages/). Site soil hydraulic properties were parameterised using Brooks and Corey (1964) relations. These properties were derived from data collected at each site or, when local data were not available, calculated from the sand/silt/clay fractions in the nearest gridbox in the high-resolution input file to the Met Office Central Ancillary Program (Dharssi *et al.*, 2009), using approximations from Cosby *et al.* (1984). The model was spun-up by recycling the meteorological data at each site for up to 50 years.

Results

SOX sensitivity to environmental and hydraulic drivers

The SOX analytical approximation (Eqn 4-5) has g_s responses to climate which are consistent with the patterns commonly reported in the literature (Mott, 1988; Leuning, 1995; Dewar *et al.*, 2018). The g_s responses to I_{par} and c_a in SOX (Fig. 1a) are given by the $\partial A/\partial c_i$ gradient decreasing at low light because of the changes in the light response curve, as A starts being limited by light (Notes S3), or at high c_a, which affects the gradient between $A(c_a)$ and $A(c_{i,col})$ (Notes S2). SOX correctly predicted stomatal closure in response to increased c_a under Rubisco-limited conditions (Mott, 1988; Fig. 1a). The classical exponential g_s responses to D (Leuning, 1995) was reproduced in SOX (Fig. 1a) through the D effect on ξ (Eqn 5; Fig. S1a). An exponential g_s decline was also predicted by SOX in response to decreasing Ψ_{pd}, (Fig. 1a) which summarizes both the responses to the soil water availability in the root zone and the hydraulic stress of transporting water to the

top of the canopy (Eqn S1.2 in Notes S1). The plant hydraulic parameters modulated the model sensitivity to D or Ψ_{pd} (Fig. 1b-d), with a less negative Ψ_{50} or a higher r_{pmin} increasing the g_s sensitivity to Ψ_{pd} and D (Fig. 1c-d). The effect of the vulnerability curve shape parameter a was more complex, lower a increased g_s sensitivity to less negative $\Psi_{pd,}$ but decreased g_s sensitivity to very negative Ψ_{pd} values (Fig. 1c).

The patterns produced by the analytical SOX were similar to the numerical version from Eller *et al.* (2018b), with a correlation coefficient ranging from 0.92 to 1 (Fig. S3). However, the use of linear gradients in equations 4 and 5 (Notes S2) can cause discrepancies between the different model versions under certain ranges of environmental conditions. The analytical version of SOX underestimated g_s at low D (Fig. S3), overestimated g_s at low c_a, and g_s increased faster in response to light (Fig. S3) than in the numerical model.

SOX leaf-level evaluation

SOX simulated the observed leaf-level g_s responses to soil drought better than the β-function in all the studied woody PFTs, except BDT (Fig. 2). The β-function predicted all PFTs will reach $g_s = 0$ at $\Psi_{pd} > -2$ MPa, whereas SOX predicted $g_s > 0$ even when $\Psi_{pd} < -4$ MPa in some PFTs (Fig. 2b, e). The less conservative stomatal behaviour predicted by SOX produced a NSE, on average, 0.65 higher and a RMSE 26% lower than the β-function. Most of the observed g_s was within SOX 95% confidence bounds derived from the hydraulic parameters' uncertainty (shaded region in Fig. 2). The only values outside SOX uncertainty boundaries were the highest g_s values in BET-Tr and BET-Te (Fig. 2a-b), and the lowest NET g_s values when $\Psi_{pd} > -3.5$ MPa (Fig. 2d).

SOX produced a better fit to the g_s data, which resulted in a lower AIC than the β-function for all PFTs, except BDT (Table 1). Fitting the two empirical parameters of the Jacobs (1994) equation (f_0 and D_{crit}, Eqn 8) to the g_s data results in a β-function AIC score 512.1 higher than SOX (Table

316 1). For the BDT observations, the β-function results in an AIC score 11.6 lower than SOX. Our
317 BDT observations were restricted to relatively well watered conditions (lowest Ψ_{pd} was -1.2 MPa),
318 which limits the utility of this dataset to evaluate the model responses to soil drought.

319 *JULES-SOX site-level calibration*

320 The hydraulic parameters that maximized the JULES-SOX fit to the GPP data at the calibration
321 sites (Table S2; Fig. S2) were within one SD of the mean observed hydraulic parameters for most
322 PFTs (Table 2). The Gymnosperm PFTs (NDT and NET) required Ψ_{50} values 1.6 MPa less
323 negative than their observed Ψ_{50} means to fit the GPP data, which is lower than the observed SD
324 range but still within the range of Ψ_{50} observations for NET (Ψ_{50} ranges from -2.3 to -7.5 MPa in
325 NET). The NDT and BET-Tr calibrated a were also slightly lower than the SD range (Table 2),
326 but within the observed a range for BET-Tr (a ranges from 1.8 to 7.8 in BET-Tr). The only PFT
327 with a calibrated r_{pmin} outside the SD range of the mean r_{pmin} was ESh (Table 2).

328 The monthly GPP modelled by JULES-SOX fitted the eddy covariance GPP data better than
329 the default JULES in 8 out of the 9 sites used for parameter calibration (Table S2; Fig. S2) (Fig.
330 3). The default JULES NSE was 0.01 higher in the DSh site (Fig. 3i), whereas in all the other sites
331 JULES-SOX had a better fit. The difference between JULES-SOX and default JULES NSE ranged
332 from 0.03 for C3 grasses (Fig. 3f) to 11.44 for BET-Tr (Fig. 3a). The large improvement in the
333 BET-Tr site was caused by the lower GPP decline predicted by SOX during Jan-Mar and Sep-Dec.
334 The decline in BET-Tr GPP in default JULES can be attributed to the β-factor overestimating the
335 effects of soil moisture on the vegetation carbon assimilation during drier periods (Fig. S4a). On
336 average, JULES-SOX NSE for GPP was 1.59 higher than default JULES, while its RMSE was
337 38% lower than JULES.

The less conservative stomatal behaviour predicted by SOX resulted in higher evapotranspiration rates throughout the year (Fig. S5; S6), which depleted soil moisture to lower levels than the β-function in default JULES during drier periods (Fig. S4; S7). The soil moisture dynamics from JULES-SOX are more closely aligned with the monthly soil moisture observations in 8 out of the 10 sites where soil moisture data was available (Fig. S7). JULES-SOX NSE for monthly soil moisture was 1.67 higher and a RMSE 19% lower than default JULES. JULES-SOX also simulates realistic Ψ_c for most PFTs (Fig. 4; S4). The modelled Ψ_c at the calibration sites is within the interquartile range of the observed minimum Ψ_c at midday for all woody PFTs, except NDT (Fig. 4).

Biome-level JULES-SOX evaluation

Using JULES-SOX with calibrated SOX hydraulic parameters produced a better fit to the GPP data than default JULES for 50 out of the 70 eddy flux evaluation sites (Table S2; Table 3; Fig. 5). Across all biomes the JULES-SOX median NSE was 0.19 higher than default JULES, and its RMSE was 19% lower (Table 3). The difference between JULES-SOX and JULES skill was highest at EBF-Tr sites, which have a median NSE 3.18 higher and RMSE 45% lower in JULES-SOX (Table 3; Fig 5a). The fit of EBT-Te to data was also improved substantially by JULES-SOX, with JULES-SOX having a median NSE 1.01 higher and a RMSE 18% lower (Fig. 5a; Table 3). Default JULES only outperformed JULES-SOX at CRO, which have a median NSE 0.08 lower in JULES-SOX, and GRA where the RMSE 5% was higher in JULES-SOX (Fig. 5a; Table 3).

Default JULES significantly underestimated the observed mean annual GPP by 143.3 g C m^{-2} across all biomes, which corresponds to 13.6% of the observed mean annual GPP (Fig. 5b). JULES-SOX deviation from the observed mean annual GPP was considerably smaller (71.6 g C m^{-2}; Fig. 5b). The significantly lower annual GPP predicted by default JULES can be attributed to

361 β-function induced GPP declines, which also produced a stronger GPP seasonality than what is
362 present in the data (Fig. 5c). JULES overestimated the median observed GPP seasonality by 70%,
363 versus a 13% overestimation by JULES-SOX (Fig. 5c). This difference means JULES predicts
364 17% of the sites have a markedly seasonal GPP (SI > 0.8; Walsh & Lawler, 1981) while just 4 %
365 of the sites actually have SI > 0.8. JULES-SOX predicts only 8% of the sites would have SI > 0.8.
366 The light use efficiency (LUE; Fig. 6) is the ratio between GPP and the I_{par} absorbed by the
367 canopy (Stocker *et al.*, 2018), and can be used to disentangle the effects of soil moisture and light
368 availability controlling the vegetation GPP. The JULES LUE declined as soil dries out with a mean
369 linear slope of 1.21 (±0.1) across all biomes. In contrast, the JULES-SOX LUE-soil moisture
370 relationship had a mean slope of 0.73 (±0.21) with some biomes, such as DBF, reaching a slope
371 as low as 0.22 (Fig. 6b). The consequence of sustaining higher LUE at low soil moisture in JULES-
372 SOX is a greater depletion of soil moisture, as indicated by the more left skewed soil moisture
373 probability distribution predicted by JULES-SOX (lower panels in Fig. 6). The mean moisture
374 content of the top 1 m of soil predicted by JULES-SOX was, on average, 10% lower than default
375 JULES. In JULES-SOX some biomes, such as ENF, could reach a soil moisture on average 17%
376 lower than JULES (Fig. 6f).

377 **Discussion**

378 We report the first evaluation of a LSM using a stomatal optimization model fully based on
379 xylem hydraulics (SOX) to drive the vegetation stomatal responses to climate. Our results provide
380 support for the SOX underlying hypothesis that stomata evolved to balance carbon assimilation
381 with instantaneous hydraulic conductance loss. The risk of mortality through hydraulic failure
382 (Choat *et al.*, 2012; Rowland *et al.*, 2015; Anderegg *et al.*, 2016; Adams *et al.*, 2017), should drive
383 the evolution of mechanisms to prevent the plant from reaching lethal embolism thresholds

(Sperry, 2004). There is abundant evidence that stomata controls xylem tension, and consequently embolism (Hubbard *et al.*, 2001; Brodribb *et al.*, 2003; Meinzer *et al.*, 2009; Klein, 2014). Our model represents this xylem-stomata coordination through the assumption of optimisation by natural selection (Wolf *et al.*, 2016).

Whereas our model fits the observations of most PFTs better than its empirical alternative, there is still a considerable amount of unexplained variance in the data (Fig. 2). This can be partially attributed to the large hydraulic heterogeneity within each PFT, but we must also acknowledge that many processes not directly related with xylem hydraulics are important to plant life history and stomatal evolution. Processes related to nutrient use and acquisition, carbohydrate allocation and storage, the maintenance of tissues and biochemical apparatus, and protection from pathogens and herbivores (Melotto *et al.,* 2008; Cramer *et al.,* 2009; Prentice *et al.,* 2014) all could explain part of our model residual variance. It is extremely important to explore the relevance of these processes in future research on stomatal optimality. However, the SOX model as we propose already provides a parsimonious alternative to the empirical models commonly used in LSM.

Our findings that xylem hydraulics-based models can adequately simulate stomatal behaviour agree with other recent studies. For example, Anderegg *et al.* (2018b) shows that a hydraulics based optimization model can simulate the stomatal behaviour of woody plants better than CF. More recently, Wang *et al.* (2019) shows that a similar hydraulics-based model can predict stomatal responses to increased CO_2 better than the Ball-Berry-Leuning empirical model (Leuning, 1995). These results show the potential of using plant hydraulics to model the stomatal behaviour of plants across contrasting environmental conditions, and supports its use in ESMs to project the evolution of global climate.

406 The analytical formulation developed for SOX facilitates its coupling to LSMs, allowing the
407 host LSM to constrain its predictions using plant hydraulic information. We show that including
408 plant hydraulics in JULES through SOX improves its capabilities to simulate GPP and soil
409 moisture dynamics in most of the studied biomes (Fig. 3-5). In addition, SOX opens new
410 possibilities to evaluate LSM predictions and expands the range of hypotheses that can be tested
411 with JULES. Using JULES-SOX within ESMs will allow us to understand how hydraulic
412 processes affect climatic and biogeochemical cycles at global scale, as well as to investigate the
413 role of plant hydraulics on vegetation distribution and its response to climate change.

414 *SOX parametrization and parsimony*

415 Other LSMs and DGVMs have already successfully employed principles of plant hydraulics
416 (Hickler *et al.*, 2006; Bonan *et al.*, 2014; Kennedy *et al.*, 2019), but JULES-SOX is the first LSM
417 to use the new generation of hydraulically-based stomatal optimization models (Wolf *et al.,* 2016;
418 Sperry *et al.,* 2017; Anderegg *et al.,* 2018b; Eller *et al.,* 2018b) to predict stomatal responses to
419 climate. The SPA (Williams *et al.*, 1996) adaptation to the Community Land Model (CLM) by
420 Bonan *et al.* (2014) was one of the first approaches to link plant stomatal function to plant hydraulic
421 processes in a LSM. Despite SPA being an extremely useful model, SOX has an advantage in
422 circumstances where assuming a strict isohydric behaviour is not appropriate (Klein, 2014;
423 Martinez-Vilalta *et al.*, 2014). In relation to SOX, SPA does not represent dynamic changes in the
424 plant hydraulic conductance or an anisohydric mode of stomatal regulation (Williams *et al.,* 1996;
425 Fisher *et al.,* 2006). However, SPA accounts for plant hydraulic capacitance, which can be
426 important for plant functioning, especially during early morning (Goldstein *et al.*, 1998), and is
427 currently not implemented in SOX.

Recently Kennedy *et al.* (2019) implemented a Plant Hydraulic Scheme (PHS) in CLM. The PHS simulates dynamic changes in hydraulic conductance in different compartments along the soil-atmosphere continuum, providing a more detailed representation than SOX of hydraulic processes occurring along the soil-plant hydraulic pathway. However, PHS still requires empirical parameters to represent stomatal responses to soil drought and *D* (Kennedy *et al.* 2019), namely the g_0 and g_1 parameters from the Medlyn *et al.* (2011) model, and the critical and wilting points used in the empirical stress factor. The main advantage of SOX is providing an alternative to the β-function and empirical stomatal parameters by linking plant hydraulic processes directly to stomatal functioning. As we treat the soil-plant-atmosphere pathway as a single hydraulic compartment, SOX only requires the hydraulic parameters r_{pmin}, Ψ_{50} and a to predict stomatal responses to climate. This makes SOX even more parsimonious than default JULES, which requires four empirical parameters to simulate stomatal responses to climate (Eqn 7-8) and does not simulate any aspect of vegetation hydraulic functioning (Clark *et al.*, 2011).

We show that the SOX hydraulic parameters in most PFTs can be constrained with plant branch-level hydraulic observations (Table 2), which is an advantage over models that employ empirical parameters difficult to constrain and interpret biologically. However, we observed discrepancies between the SOX-calibrated parameters and the observed hydraulic traits in certain PFTs (Table 2). In some cases, such as NDT, the parameter discrepancy may have been due to a very restricted observational sampling of hydraulic parameters in this group. The NDT only had Ψ_{50} data for five species and a and r_{pmin} for two species (Table 2). Considering that the observations used in this study were not collected in the same FLUXNET sites used to evaluate SOX, some of the observed discrepancies between calibrated and measured parameters might reflect hydraulic differences between populations treated as the same PFT in this study. For example, the deciduous

angiosperms species present in the XFT dataset used in this study contain mostly hydraulic data from cold-deciduous temperate species (Mencuccini *et al.,* 2019b), which might not be adequate to describe the hydraulic system of tropical and subtropical drought-deciduous. Our hydraulic scheme opens possibilities to improve the representation of different global vegetation types in JULES with different hydraulic and phenological strategies. Capturing the large diversity of ecological strategies in plants is important to simulate species rich ecosystems such as tropical forests (Xu *et al.,* 2016).

Anderegg *et al.* (2018a) computed the community weighted average values for Ψ_{50} in two of the FLUXNET sites used in this study (US-MMS and IT-Ren) and obtained values closer to the calibrated values for BDT and NET (-2.1 and -3.6 MPa, respectively), than the means from our compiled hydraulic dataset (Table 2). In Eller *et al.* (2018b) a numerical version of SOX outperformed the β-function approach when parameterized with locally measured branch-level hydraulic data from EBF-Tr. These findings suggest that SOX can be constrained with *in-situ* hydraulic measurements when these are available. However, we must also consider the possibility that there are intrinsic limitations in using branch-level hydraulic data to parameterize the model. Roots and leaves can be more vulnerable to embolism than branches (Bartlett *et al.*, 2016; Wolfe *et al.*, 2016), which can make these tissues bottleneck plant hydraulic conductance during drought. The soil outside the roots can also limit plant hydraulic conductance and, ultimately, control its water use (Fisher *et al*. 2007). These bottlenecks could bias the SOX calibrated hydraulic parameters towards the limiting component and explain its departure from the branch-level hydraulic data. In this case SOX parameterization would benefit from the use of more integrative methodologies to estimate hydraulic parameters that represent the entire soil-plant hydraulic vulnerability (Eller *et al.*, 2018a). Alternatively, the SOX structure (i.e., the *K* function in Eqn 2)

would need to explicitly represent the variability between different hydraulic compartments along the soil-plant-atmosphere pathway, similarly to SPA or other models (Kennedy *et al.,* 2019; Mencuccini *et al.,* 2019b; Eller *et al.*, 2018b).

Ecosystem-level implications of SOX

SOX improved JULES GPP simulation in over 70% of the 70 studied sites and soil moisture dynamics in 80% of the 10 sites where soil moisture data were available. This improved fit was achieved using hydraulic parameters calibrated against the GPP data of a small subset of eddy flux sites (the sites in Fig. S2), which suggests that the calibrated parameters are generic enough to be used in global simulations. The lower sensitivity of SOX to soil moisture improved the simulations of annual GPP (Fig. 5) and predicted terrestrial biomes to assimilate on average 2.58 Mg C ha^{-1} yr^{-1} or 30% more than predicted by default JULES. This increased carbon assimilation could affect Earth's atmospheric CO_2 evolution and climate change projections (Cox *et al.*, 2000; Winkler *et al.*, 2019) .

JULES-SOX particularly improved the fit of EBF-Tr sites to the observations (Fig. 5; Table 3), using hydraulic parameters very similar to those observed in BET-Tr (Table 2). Considering that SOX is also able to capture the response of EBF-Tr even to extreme experimental drought (Eller *et al.*, 2018b), JULES-SOX may contribute to decrease the large uncertainty in how these important ecosystems will respond to climate change (Sitch *et al.*, 2008). Tropical forest productivity estimated by SOX is less sensitive to seasonal soil drought (Fig. 3; S4), which is consistent with the little seasonality often observed in tropical forest-atmosphere CO_2 exchange (Grace *et al.*, 1995; Carswell *et al.*, 2002; Alden *et al.*, 2016), as well as to forest responses to experimental drought (Meir *et al.*, 2009; da Costa *et al.*, 2010; Meir *et al.*, 2018). da Costa *et al.* (2018) shows that even after 15 years of partial rainfall exclusion, Amazon trees can maintain or

even increase their transpiration rates (albeit following significant mortality). Whereas tropical forest resistance to drought has previously been attributed only to deep roots possessed by the vegetation (Nepstad *et al.*, 1994), our results indicate that plants more resistant to embolism could maintain their carbon assimilation during drought even without a deeper root system.

The unavoidable consequence of maintaining stomatal gas exchange during soil drought is a greater depletion of soil moisture reserves (Fig. 6; S4; S7). This behaviour is a direct consequence of the main assumption in SOX, which reflects a 'use or lose it' stomatal regulation strategy with respect to soil moisture (Sperry et al., 2017). SOX assumes plants with a more conservative water use strategy will be outcompeted by neighbouring plants with a less conservative stomatal behaviour (Wolf *et al.* 2016). The demographic consequences of the stomatal regulation strategy embedded in SOX should be explored in future studies using the dynamic vegetation component of JULES (Cox, 2001; Moore *et al.*, 2018). The more competitive soil moisture dynamics predicted by SOX, together with a more accurate representation of vegetation drought-induced mortality, which also can be developed from SOX, might be the key to predict sudden and widespread vegetation die-off during droughts that have been increasingly reported in ecosystems around the globe (Allen *et al.*, 2010; Worrall *et al.*, 2010; Meir *et al.*, 2015).

Acknowledgments

This research was supported by the Newton Fund through the Met Office Climate Science for Service Partnership Brazil (CSSP Brazil) and a NERC independent fellowship grant NE/N014022/1 to LR. This work used eddy covariance data acquired and shared by the FLUXNET community, including these networks: AmeriFlux, AfriFlux, AsiaFlux, CarboAfrica, CarboEuropeIP, CarboItaly, CarboMont, ChinaFlux, Fluxnet-Canada, GreenGrass, ICOS, KoFlux, LBA, NECC, OzFlux-TERN, TCOS-Siberia, and USCCC. The ERA-Interim reanalysis

data are provided by ECMWF and processed by LSCE. The FLUXNET eddy covariance data processing and harmonization was carried out by the European Fluxes Database Cluster, AmeriFlux Management Project, and Fluxdata project of FLUXNET, with the support of CDIAC and ICOS Ecosystem Thematic Center, and the OzFlux, ChinaFlux and AsiaFlux offices.

Author contribution

CBE, LR, MM, SS and PMC led the scientific development of SOX. PMC and CBE derived the analytical solution. CBE evaluated leaf-level SOX using data provided by LR, PM, MM, TR, BM, YW, TK, GST, RSO, ISM, BHPR. CBE and KW coded SOX into JULES. KW and AH created a JULES suite used by CBE to evaluate JULES-SOX against eddy covariance data collected by KF, GW, LM, among other FLUXNET and LBA PIs. All authors contributed to writing the manuscript.

References

Adams HD, Zeppel MJB, Anderegg WRL, Hartmann H, Landhäusser SM, Tissue DT, Huxman TE, Hudson PJ, Franz TE, Allen CD, *et al.* 2017. A multi-species synthesis of physiological mechanisms in drought-induced tree mortality. *Nature Ecology and Evolution* **1**: 1285–1291.

Alden CB, Miller JB, Gatti L V., Gloor MM, Guan K, Michalak AM, van der Laan-Luijkx IT, Touma D, Andrews A, Basso LS, *et al.* 2016. Regional atmospheric CO2 inversion reveals seasonal and geographic differences in Amazon net biome exchange. *Global change biology* **22**: 3427–3443.

Allen CD, Macalady AK, Chenchouni H, Bachelet D, McDowell N, Vennetier M, Kitzberger T, Rigling A, Breshears DD, Hogg EH (Ted., *et al.* 2010. A global overview of drought and heat-induced tree mortality reveals emerging climate change risks for forests. *Forest Ecology and Management* **259**: 660–684.

Anderegg WRL, Klein T, Bartlett M, Sack L, Pellegrini AFA, Choat B, Jansen S. 2016. Meta-analysis reveals that hydraulic traits explain cross-species patterns of drought-induced tree mortality across the globe. *Proceedings of the National Academy of Sciences* **113**: 5024–5029.

Anderegg WRL, Konings AG, Trugman AT, Yu K, Bowling DR, Gabbitas R, Karp DS, Pacala S, Sperry JS, Sulman BN, *et al.* 2018a. Hydraulic diversity of forests regulates

548 ecosystem resilience during drought. *Nature* **561**: 538.
549 **Anderegg WRL, Trugman AT, Bowling DR, Salvucci G, Tuttle SE**. **2019**. Plant functional
550 traits and climate influence drought intensification and land–atmosphere feedbacks. *Proceedings*
551 *of the National Academy of Sciences of the United States of America* **116**: 14071–14076.
552 **Anderegg WRL, Wolf A, Arango-Velez A, Choat B, Chmura DJ, Jansen S, Kolb T, Li S,**
553 **Meinzer FC, Pita P, *et al.* 2018b**. Woody plants optimise stomatal behaviour relative to
554 hydraulic risk. *Ecology Letters* **21**: 968-977.
555 **Baldocchi D, Falge E, Gu L, Olson R, Hollinger D, Running S, Anthoni P, Bernhofer C,**
556 **Davis K, Evans R, *et al.* 2001**. FLUXNET: A New Tool to Study the Temporal and Spatial
557 Variability of Ecosystem-Scale Carbon Dioxide, Water Vapor, and Energy Flux Densities.
558 *Bulletin of the American Meteorological Society* **82**: 2415–2434.
559 **Bartlett MK, Klein T, Jansen S, Choat B, Sack L**. **2016**. The correlations and sequence of
560 plant stomatal, hydraulic, and wilting responses to drought. *Proceedings of the National*
561 *Academy of Sciences* **113**: 13098–13103.
562 **Berninger F, Hari P**. **1993**. Optimal regulation of gas exchange: Evidence from field data.
563 *Annals of Botany* **71**: 135–140.
564 **Best MJ, Pryor M, Clark DB, Rooney GG, Essery R, Ménard CB, Edwards JM, Hendry**
565 **MA, Porson A, Gedney N**. **2011**. The Joint UK Land Environment Simulator (JULES), model
566 description–Part 1: energy and water fluxes. *Geoscientific Model Development* **4**: 677–699.
567 **Bonan GB, Williams M, Fisher RA, Oleson KW**. **2014**. Modeling stomatal conductance in the
568 earth system: Linking leaf water-use efficiency and water transport along the soil-plant-
569 atmosphere continuum. *Geoscientific Model Development* **7**: 2193–2222.
570 **Bozdogan H**. **1987**. Model selection and Akaike's Information Criterion (AIC): The general
571 theory and its analytical extensions. *Psychometrika* **52**: 345–370.
572 **Brodribb TJ, Holbrook NM, Edwards EJ, Gutiérrez M V. 2003**. Relations between stomatal
573 closure, leaf turgor and xylem vulnerability in eight tropical dry forest trees. *Plant, Cell and*
574 *Environment* **26**: 443–450.
575 **Buckley TN**. **2017**. Modeling Stomatal Conductance. *Plant Physiology* **174**: 572–582.
576 **Buckley TN. 2019.** How do stomata respond to water status? *New Phytologist* **224**: 21-36.
577 **Carswell FE, Costa AL, Palheta M, Malhi Y, Meir P, Costa JDPR, Ruivo MDL, Leal**
578 **LDSM, Costa JMN, Clement RJ, *et al.* 2002**. Seasonality in CO2 and H2O flux at an eastern

Amazonian rain forest. *Journal of Geophysical Research D: Atmospheres* **107**: LBA-43.

Choat B, Brodribb TJ, Brodersen CR, Duursma RA, López R, Medlyn BE. **2018**. Triggers of tree mortality under drought. *Nature* **558**: 531–539.

Choat B, Jansen S, Brodribb TJ, Cochard H, Delzon S, Bhaskar R, Bucci SJ, Feild TS, Gleason SM, Hacke UG, *et al.* 2012. Global convergence in the vulnerability of forests to drought. *Nature* **491**: 752–755.

Clark DB, Mercado LM, Sitch S, Jones CD, Gedney N, Best MJ, Pryor M, Rooney GG, Essery RLH, Blyth E, *et al.* 2011. The Joint UK Land Environment Simulator (JULES), Model description – Part 2: Carbon fluxes and vegetation. *Geoscientific Model Development Discussions* **4**: 641–688.

Cosby BJ, Hornberger GM, Clapp RB, Ginn TR. **1984**. A Statistical Exploration of the Relationships of Soil Moisture Characteristics to the Physical Properties of Soils. *Water Resources Research* **20**: 682–690.

da Costa ACL, Galbraith D, Almeida S, Portela BTT, da Costa M, de Athaydes Silva Junior J, Braga AP, de Gonçalves PHL, de Oliveira AA, Fisher R, *et al.* 2010. Effect of 7 yr of experimental drought on vegetation dynamics and biomass storage of an eastern Amazonian rainforest. *New Phytologist* **187**: 579–591.

da Costa ACL, Rowland L, Oliveira RS, Oliveira AAR, Binks OJ, Salmon Y, Vasconcelos SS, Junior JAS, Ferreira L V., Poyatos R, *et al.* 2018. Stand dynamics modulate water cycling and mortality risk in droughted tropical forest. *Global Change Biology* **24**: 249–258.

Cowan IR. **1986**. Economics of carbon fixation in higher plants. In: On the economy of plant form and function: proceedings of the Sixth Maria Moors Cabot Symposium, Evolutionary Constraints on Primary Productivity, Adaptive Patterns of Energy Capture in Plants, Harvard Forest, August 1983. Cambridge [Cambridgeshire]: Cambridge University Press, c1986.

Cowan I. **2002**. Fit, fitter, fittest; where does optimisation fit in? *Silva Fennica* **36**: 745–754.

Cowan IR, Farquhar GD. **1977**. Stomatal function in relation to leaf metabolism and environment. *Symposia of the Society for Experimental Biology* **31**: 471–505.

Cox PM. **2001**. Description of the " TRIFFID " Dynamic Global Vegetation Model. *Hadley Centre technical note*.

Cox PM, Betts RA, Jones CD, Spall SA, Totterdell IJ. **2000**. Acceleration of global warming due to carbon-cycle feedbacks in a coupled climate model. *Nature* **408**: 184.

Cox PM, Huntingford C, Harding RJ. **1998**. A canopy conductance and photosynthesis model for use in a GCM land surface scheme. *Journal of Hydrology* **212–213**: 79–94.

Cramer MD, Hawkins HJ, Verboom GA. 2009. The importance of nutritional regulation of plant water flux. *Oecologia* **161**:15-24.

Dewar RC, Franklin O, Mäkelä A, McMurtrie RE, Valentine HT. **2009**. Optimal Function Explains Forest Responses to Global Change. *BioScience* **59**: 127-139.

Dewar R, Mauranen A, Mäkelä A, Hölttä T, Medlyn B, Vesala T. **2018**. New insights into the covariation of stomatal, mesophyll and hydraulic conductances from optimization models incorporating nonstomatal limitations to photosynthesis. *New Phytologist* **217**: 571–585.

Dharssi I, Vidale PL, Verhoef A, Macpherson B, Jones C, Best M. **2009**. New soil physical properties implemented in the Unified Model at PS18. *Met Office technical report* **528**.

Duffy PB, Brando P, Asner GP, Field CB. **2015**. Projections of future meteorological drought and wet periods in the Amazon. *Proceedings of the National Academy of Sciences* **112**: 13172–13177.

Eller CB, Bittencourt PRL, Oliveira RS. **2018a**. Using sap flow to measure whole-tree hydraulic conductance loss in response to drought. *Acta Horticulturae* **1222**: 75–84.

Eller CB, Rowland L, Oliveira RS, Bittencourt PRL, Barros F V., da Costa ACL, Meir P, Friend AD, Mencuccini M, Sitch S, *et al.* 2018b. Modelling tropical forest responses to drought and El Niño with a stomatal optimization model based on xylem hydraulics. *Philosophical transactions of the Royal Society of London. Series B, Biological sciences* **373**: 20170315.

Farquhar G, Schulze E, Kuppers M. **1980**. Responses to Humidity by Stomata of Nicotiana glauca L. And Corylus avellana L. Are Consistent With the Optimization of Carbon Dioxide Uptake With Respect to Water Loss. *Australian Journal of Plant Physiology* **7**: 315–327.

Fisher RA, Williams M, Do Vale RL, Da Costa AL, Meir P. **2006**. Evidence from Amazonian forests is consistent with isohydric control of leaf water potential. *Plant, Cell and Environment* **20**: 151–165.

Friend AD. **1995**. PGEN : an integrated model of leaf photosynthesis , and conductance. *Ecological Modelling* **77**: 233–255.

Friend AD, Cox PM. **1995**. Modelling the effects of atmospheric C02 on vegetation-atmosphere interactions. *Agricultural and Forest Meteorology* **73**: 295.

Goldstein G, Andrade JL, Meinzer FC, Holbrook NM, Cavelier J, Jackson P, Celis A. **1998**. Stem water storage and diurnal patterns of water use in tropical forest canopy trees. *Plant, Cell and Environment* **21**: 397-406.

Goulden ML, Miller SD, Da Rocha HR, Menton MC, De Freitas HC, E Silva Figueira AM, Dias De Sousa CA. **2004**. Diel and seasonal patterns of tropical forest CO2 exchange. *Ecological Applications* **14**: 42–54.

Grace J, Lloyd J, McIntyre J, Miranda AC, Meir P, Miranda HS, Nobre C, Moncrieff J, Massheder J, Malhi Y, *et al.* 1995. Carbon dioxide uptake by an undisturbed tropical rain forest in Southwest Amazonia, 1992 to 1993. *Science* **270**: 778–780.

Harper AB, Cox PM, Friedlingstein P, Wiltshire AJ, Jones CD, Sitch S, Mercado LM, Groenendijk M, Robertson E, Kattge J, *et al.* 2016. Improved representation of plant functional types and physiology in the Joint UK Land Environment Simulator (JULES v4.2) using plant trait information. *Geoscientific Model Development* **9**: 2415–2440.

Hartmann H, Moura CF, Anderegg WRL, Ruehr NK, Salmon Y, Allen CD, Arndt SK, Breshears DD, Davi H, Galbraith D, *et al.* 2018. Research frontiers for improving our understanding of drought-induced tree and forest mortality. *New Phytologist* **218**: 15–28.

Hickler T, Prentice IC, Smith B, Sykes MT, Zaehle S. **2006**. Implementing plant hydraulic architecture within the LPJ Dynamic Global Vegetation Model. *Global Ecology and Biogeography* **15**: 567–577.

Hubbard RM, Ryan MG, Stiller V, Sperry JS. **2001**. Stomatal conductance and photosynthesis vary linearly with plant hydraulic conductance in ponderosa pine. *Plant, Cell and Environment* **24**: 113–121.

Jacobs C. **1994**. Direct impact of atmospheric CO2 enrichment on regional transpiration.

Kattge J, Díaz S, Lavorel S, Prentice IC, Leadley P, Bönisch G, Garnier E, Westoby M, Reich PB, Wright IJ, *et al.* 2011. TRY - a global database of plant traits. *Global Change Biology* **17**: 2905–2935.

Kennedy D, Swenson S, Oleson KW, Lawrence DM, Fisher R, Costa ACL da, Gentine P. **2019**. Implementing plant hydraulics in the Community Land Model, version 5. *Journal of Advances in Modeling Earth Systems* **11**: 485-513.

Klein T. **2014**. The variability of stomatal sensitivity to leaf water potential across tree species indicates a continuum between isohydric and anisohydric behaviours. *Functional Ecology* **28**:

1313–1320.

Lens F, Picon-Cochard C, Delmas CEL, Signarbieux C, Buttler A, Cochard H, Jansen S, Chauvin T, Doria LC, Del Arco M, *et al.* 2016. Herbaceous angiosperms are not more vulnerable to drought-induced embolism than angiosperm trees. *Plant Physiology* **172**: 661–667.

Leuning R. **1995**. A critical appraisal of a combined stomatal - photosynthesis model for C3 plants. *Plant, Cell & Environment* **18**: 339–355.

Lin Y, Medlyn B, Duursma R. **2015**. Optimal stomatal behaviour around the world. *Nature Climate Change* **5**: 459.

Loveland TR, Reed BC, Ohlen DO, Brown JF, Zhu Z, Yang L, Merchant JW. **2000**. Development of a global land cover characteristics database and IGBP DISCover from 1 km AVHRR data. *International Journal of Remote Sensing* **21**: 1303–1330.

Mäkelä A, Berninger F, Hari P. **1996**. Optimal control of gas exchange during drought: Theoretical analysis. *Annals of Botany* **77:** 461-468.

Melotto M, Underwood W, He SY. 2008. Role of stomata in plant innate immunity and foliar bacterial diseases. *Annual Review of Phytopathology* **46**: 101-122.

Manzoni S, Vico G, Palmroth S, Porporato A, Katul G. **2013**. Optimization of stomatal conductance for maximum carbon gain under dynamic soil moisture. *Advances in Water Resources* **62**: 90–105.

Marengo JA, Souza CM, Thonicke K, Burton C, Halladay K, Betts RA, Alves LM, Soares WR. **2018**. Changes in Climate and Land Use Over the Amazon Region: Current and Future Variability and Trends. *Frontiers in Earth Science* **6**: 228.

Martinez-Vilalta J, Poyatos R, Aguade D, Retana J, Mencuccini M. **2014**. A new look at water transport regulation in plants. *New Phytologist* **204**: 105–115.

Medlyn BE, Barton CVM, Broadmeadow MSJ, Ceulemans R, De Angelis P, Forstreuter M, Freeman M, Jackson SB, Kellomäki S, Laitat E, *et al.* 2001. Stomatal conductance of forest species after long-term exposure to elevated CO2 concentration: A synthesis. *New Phytologist* **149**: 247–264.

Medlyn BE, Duursma RA, Eamus D, Ellsworth DS, Prentice IC, Barton CVM, Crous KY, De Angelis P, Freeman M, Wingate L. **2011**. Reconciling the optimal and empirical approaches to modelling stomatal conductance. *Global Change Biology* **17**: 2134–2144.

Medlyn BE, De Kauwe MG, Zaehle S, Walker AP, Duursma RA, Luus K, Mishurov M,

Pak B, Smith B, Wang YP, *et al.* 2016. Using models to guide field experiments: a priori predictions for the CO2 response of a nutrient- and water-limited native Eucalypt woodland. *Global change biology* **22**: 2834–2851.

Medlyn BE, Zaehle S, De Kauwe MG, Walker AP, Dietze MC, Hanson PJ, Hickler T, Jain AK, Luo Y, Parton W, *et al.* 2015. Using ecosystem experiments to improve vegetation models. *Nature Climate Change* **5**: 528.

Meinzer FC, Johnson DM, Lachenbruch B, McCulloh K a, Woodruff DR. **2009**. Xylem hydraulic safety margins in woody plants: Coordination of stomatal control of xylem tension with hydraulic capacitance. *Functional Ecology* **23**: 922–930.

Meir P, Brando PM, Nepstad D, Vasconcelos S, Costa ACL, Davidson E, Almeida S, Fisher RA, Sotta ED, Zarin D, *et al.* 2009. *Amazonia and Global Change* (J Gash, M Keller, M Bustamante, and P Silva Dias, Eds.). American Geophysical Union.

Meir P, Wood TE, Galbraith DR, Brando PM, Da Costa ACL, Rowland L, Ferreira L V. 2015. Threshold Responses to Soil Moisture Deficit by Trees and Soil in Tropical Rain Forests: Insights from Field Experiments. *BioScience* **65**: 882–892.

Meir P, Mencuccini M, Binks O, da Costa AL, Ferreira L, *et al.* 2018. Short-term effects of drought on tropical forest do not fully predict impacts of repeated or long-term drought: gas exchange versus growth. *Philosophical Transactions of the Royal Society B: Biological Sciences*, **373**(1760): 20170311.

Mencuccini M, Manzoni S, Christoffersen B. **2019a**. Modelling water fluxes in plants: from tissues to biosphere. *New Phytologist* **222**: 1207–1222.

Mencuccini M, Rosas T, Rowland L, Choat B, Cornelissen JHC, Jansen S, Kramer K, Lepenas A, Manzoni S, Niinemets U, Reich P, Schrodt F, Soudzilovskaia NA, Wright I, Martinez-Vilalta J, 2019b. Leaf economics and xylem hydraulics drive leaf/wood area ratios. *New Phytologist* doi.org/10.1111/nph.15998.

Mercado LM, Bellouin N, Sitch S, Boucher O, Huntingford C, Wild M, Cox PM. **2009**. Impact of changes in diffuse radiation on the global land carbon sink. *Nature* **458**: 1014.

Mercado LM, Huntingford C, Gash JHC, Cox PM, Jogireddy V. **2007**. Improving the representation of radiation interception and photosynthesis for climate model applications. *Tellus, Series B: Chemical and Physical Meteorology* **59**: 553–565.

Moore JR, Zhu K, Huntingford C, Cox PM. **2018**. Equilibrium forest demography explains

the distribution of tree sizes across North America. *Environmental Research Letters* **13**: 084019.

Mott KA. **1988**. Do Stomata Respond to CO2 Concentrations Other than Intercellular? *Plant Physiology* **86**: 200–203.

Nash JE, Sutcliffe JV. **1970**. River flow forecasting through conceptual models part I — A discussion of principles. *Journal of Hydrology* **10**: 282–290.

Nepstad DC, De Carvalho CR, Davidson EA, Jipp PH, Lefebvre PA, Negreiros GH, Da Silva ED, Stone TA, Trumbore SE, Vieira S. **1994**. The role of deep roots in the hydrological and carbon cycles of Amazonian forests and pastures. *Nature* **372**: 666–669.

Ocheltree TW, Nippert JB, Prasad PVV. **2016**. A safety vs efficiency trade-off identified in the hydraulic pathway of grass leaves is decoupled from photosynthesis, stomatal conductance and precipitation. *New Phytologist* **210**: 97–107.

Oliveira RS, Costa FRC, van Baalen E, de Jonge A, Bittencourt PR, Almanza Y, Barros F de V., Cordoba EC, Fagundes M V., Garcia S, *et al.* 2019. Embolism resistance drives the distribution of Amazonian rainforest tree species along hydro-topographic gradients. *New Phytologist* **221**: 1457–1465.

Powell TL, Galbraith DR, Christoffersen BO, Harper A, Imbuzeiro HMA, Rowland L, Almeida S, Brando PM, da Costa ACL, Costa MH, *et al.* 2013. Confronting model predictions of carbon fluxes with measurements of Amazon forests subjected to experimental drought. *New Phytologist* **200**: 350–365.

Prentice IC, Dong N, Gleason SM, Maire V, Wright IJ. 2014. Balancing the costs of carbon gain and water transport: testing a new theoretical framework for plant functional ecology. *Ecology letters* **17**: 82-91.

Qu X, Cao B, Kang J, Wang X, Han X, Jiang W, *et al.* 2019. Fine-tuning stomatal movement through small signaling peptides. *Frontiers in plant science* **10**: 69.

Restrepo-Coupe N, Levine NM, Christoffersen BO, Albert LP, Wu J, Costa MH, Galbraith D, Imbuzeiro H, Martins G, da Araujo AC, *et al.* 2017. Do dynamic global vegetation models capture the seasonality of carbon fluxes in the Amazon basin? A data-model intercomparison. *Global Change Biology* **23**: 191–208.

Rogers A, Medlyn BE, Dukes JS, Bonan G, von Caemmerer S, Dietze MC, Kattge J, Leakey ADB, Mercado LM, Niinemets U, *et al.* 2017. A roadmap for improving the representation of photosynthesis in Earth system models. *New Phytologist* **213**: 22–42.

Rowland L, Da Costa ACL, Galbraith DR, Oliveira RS, Binks OJ, Oliveira AAR, Pullen AM, Doughty CE, Metcalfe DB, Vasconcelos SS, *et al.* 2015. Death from drought in tropical forests is triggered by hydraulics not carbon starvation. *Nature* **528**: 119–122.

Saleska SR, da Rocha HR, Huete AR, Nobre AD, Artaxo P, Shimabukuro YE. 2013. LBA-ECO CD-32 Flux Tower Network Data Compilation, Brazilian Amazon: 1999-2006. Data set. *Oak Ridge National Laboratory Distributed Active Archive Center, Oak Ridge, Tennessee, USA*.

Savage VM, Bentley LP, Enquist BJ, Sperry JS, Smith DD, Reich PB, von Allmen EI. 2010. Hydraulic trade-offs and space filling enable better predictions of vascular structure and function in plants. *Proceedings of the National Academy of Sciences of the United States of America* **107**: 22722–22727.

Sellers PJ. 1985. Canopy reflectance, photosynthesis and transpiration. *International Journal of Remote Sensing* **6**: 1335–1372.

Sheffield J, Wood EF. 2008. Projected changes in drought occurrence under future global warming from multi-model, multi-scenario, IPCC AR4 simulations. *Climate Dynamics* **31**: 79–105.

Sitch S, Huntingford C, Gedney N, Levy PE, Lomas M, Piao SL, Betts R, Ciais P, Cox P, Friedlingstein P, *et al.* 2008. Evaluation of the terrestrial carbon cycle, future plant geography and climate-carbon cycle feedbacks using five Dynamic Global Vegetation Models (DGVMs). *Global Change Biology* **14**: 2015–2039.

Sperry JS. 2004. Coordinating stomatal and xylem functioning–an evolutionary perspective. *New Phytologist* **162:** 568-570.

Sperry JS, Venturas MD, Anderegg WRL, Mencuccini M, Mackay DS, Wang Y, Love DM. 2017. Predicting stomatal responses to the environment from the optimization of photosynthetic gain and hydraulic cost. *Plant Cell and Environment* **40**: 816–830.

Stocker BD, Zscheischler J, Keenan TF, Prentice IC, Peñuelas J, Seneviratne SI. 2018. Quantifying soil moisture impacts on light use efficiency across biomes. *New Phytologist* **218**: 1430–1449.

Ukkola AM, De Kauwe MG, Pitman AJ, Best MJ, Abramowitz G, Haverd V, Decker M, Haughton N. 2016. Land surface models systematically overestimate the intensity, duration and magnitude of seasonal-scale evaporative droughts. *Environmental Research Letters* **11**: 104012.

Venturas MD, Sperry JS, Love DM, Frehner EH, Allred MG, Wang Y, Anderegg WRL.

2018. A stomatal control model based on optimization of carbon gain versus hydraulic risk predicts aspen sapling responses to drought. *New Phytologist* **220**: 835–850.

Walsh RPD, Lawler DM. **1981**. Rainfall Seasonality: Description, Spatial Patterns and Change Through Time. *Weather* **36**: 201–208.

Wang Y, Sperry JS, Venturas MD, Trugman AT, Love DM, Anderegg WR. 2019. The stomatal response to rising CO2 concentration and drought is predicted by a hydraulic trait-based optimization model. *Tree Physiology*.

Williams M, Rastetter EB, Fernandes DN, Goulden ML, Wofsy SC, Shaver GR, Melillo JM, Munger JW, Fan SM, Nadelhoffer KJ. **1996**. Modelling the soil-plant-atmosphere continuum in a Quercus-acer stand at Harvard forest: The regulation of stomatal conductance by light, nitrogen and soil/plant hydraulic properties. *Plant, Cell and Environment* **19**: 911–927.

Winkler AJ, Myneni RB, Alexandrov GA, Brovkin V. **2019**. Earth system models underestimate carbon fixation by plants in the high latitudes. *Nature Communications* **10**.

Wolf A, Anderegg WRL, Pacala SW. **2016**. Optimal stomatal behavior with competition for water and risk of hydraulic impairment. *Proceedings of the National Academy of Sciences* **113**: E7222–E7230.

Wolfe BT, Sperry JS, Kursar TA. **2016**. Does leaf shedding protect stems from cavitation during seasonal droughts? A test of the hydraulic fuse hypothesis. *New Phytologist* **212**: 1007–1018.

Worrall JJ, Marchetti SB, Egeland L, Mask RA, Eager T, Howell B. **2010**. Effects and etiology of sudden aspen decline in southwestern Colorado, USA. *Forest Ecology and Management* **260**: 638–648.

Xu X, Medvigy D, Powers JS, Becknell JM, Guan K. 2016. Diversity in plant hydraulic traits explains seasonal and inter-annual variations of vegetation dynamics in seasonally dry tropical forests. *New Phytologist* **212**: 80-95.

827
828
829
830
831
832

833 **Figure captions.**

834 **Figure 1.** SOX stomatal conductance (g_s) sensitivity to environmental drivers in **(a)** (vapour
835 pressure deficit, D; pre-dawn water potential, Ψ_{pd}, Incident photosynthetically active radiation, I_{par},
836 and atmospheric CO_2 partial pressure, c_a) and plant hydraulic traits in **(b)** (Ψ when plant loses 50%
837 of its maximum conductance, Ψ_{50}; shape of vulnerability function, a; and minimum plant hydraulic
838 resistance, r_{pmin}). The variables were changed individually while the others were held constant at
839 their reference values (D = 0.5 kPa, Ψ_{pd} = -0.5 MPa, I_{par} = 600 µmol m^{-2} s^{-1}, c_a = 36 Pa, Ψ_{50} = -2
840 MPa, a = 3, r_{pmin} =1 m^2 s MPa $mmol^{-1}$). For the panels **(c)** and **(d)** the reference lines (dashed
841 black) represents values of Ψ_{50} = -3 MPa, a = 5, r_{pmin} =1 $mmol^{-1}$ m^2 s MPa, the coloured lines show
842 how changing each hydraulic parameter affects g_s response to Ψ_{pd} and D. The I_{par} was set to 2000
843 µmol m^{-2} s^{-1} in panels **(c)** and **(d)**. The V_{cmax25} was set to 100 µmol m^{-2} s and the rest of the
844 photosynthetic parameters follow the BET-Tr parameterization from Harper *et al.* (2016).

845 **Figure 2.** Predicted and observed (grey points) stomatal conductance (g_s) response to changes in
846 leaf pre-dawn water potential (Ψ_{pd}) for the woody plant functional types (PFT) from Harper *et al.*
847 (2016), except for Needleleaf deciduous trees which was not present in the dataset used in this
848 study. The red lines are SOX and β-function (Eqn 7-8) best fit. The shaded regions are non-
849 parametric 95% confidence boundaries derived from 1000 bootstrapping replications of the SOX
850 hydraulic inputs. All environmental conditions except Ψ_{pd} were held constant at their median
851 values when the g_s measurements were taken. The Ψ_{pd} was transformed in soil volumetric water

content to drive the β-function using Clapp & Hornberger (1978) equations parameterized with soil physical properties derived from the Met Office Central Ancillary Program (Dharssi *et al.*, 2009). The model fit to data is shown as the root mean squared errors (RMSE) and Nash-Sutcliffe (1970) model efficiency index (NSE). The PFT abbreviations are: BET-Tr (Broadleaf evergreen tropical tree), BET-Te (Broadleaf evergreen temperate tree), BDT (Broadleaf deciduous tree), NET (Needleleaf evergreen tree), ESh (Evergreen shrubs) and DSh (Deciduous shrubs).

Figure 3. Monthly mean gross primary production (GPP) modelled by default JULES (blue line) and JULES-SOX (red line) versus observations (grey points are means and bars are 2xSE) at each eddy flux site used for calibrating the SOX hydraulic parameters (PFT; Table S2 and Fig. S3). The model fit to data is shown as the root mean squared errors (RMSE) and Nash-Sutcliffe (1970) model efficiency index (NSE). The PFT abbreviations are: BET-Tr (Broadleaf evergreen tropical tree), BET-Te (Broadleaf evergreen temperate tree), BDT (Broadleaf deciduous tree), NET (Needleleaf evergreen tree), NDT (Needleleaf deciduous tree), C_3 (C_3 grasses), C_4 (C_4 grasses), ESh (Evergreen shrubs) and DSh (Deciduous shrubs).

Figure 4. Minimum observed midday leaf water potential (Ψ_{midday}) from 279 woody plant species compiled from the literature grouped using the Harper *et al.* (2016) plant functional types (PFT) categories. The SOX modelled Ψ_{midday} for each of the calibration sites (see Table S2 and Fig. S2) is plotted in red. The circle is the mean Ψ_{midday} and the arrows indicate the minimum and maximum Ψ_{midday}. The data for the deciduous PFT was restricted to the growing season. The PFT abbreviations are: BET-Tr (Broadleaf evergreen tropical tree), BET-Te (Broadleaf evergreen temperate tree), BDT (Broadleaf deciduous tree), NET (Needleleaf evergreen tree), NDT (Needleleaf deciduous tree), C_3 (C_3 grasses), C_4 (C_4 grasses), ESh (Evergreen shrubs) and DSh (Deciduous shrubs).

875 **Figure 5.** The Taylor diagram **(a)** shows the difference in JULES and JULES-SOX skill to predict
876 the monthly GPP in each biome. Green lines are the model centered root mean squared errors
877 (RMSE), points closer to the reference circle in the x-axis indicate higher model skill. The two
878 arrows highlight the improvement in model skill for EBF-Tr and EBF-Te. The boxplot panels
879 show the differences between models (default JULES in blue and JULES-SOX in red) and
880 observations in the annual gross primary productivity (GPP in **b**) and the GPP seasonality (GPP
881 SI in **c**). Data gaps were excluded from the annual GPP calculations for both models and
882 observations, therefore the differences can be used to evaluate the model skill, but the absolute
883 values do not represent the total annual GPP in each biome. The GPP SI was computed using the
884 approach from Walsh and Lawler (1981). Boxes filled with lines are different (at α=0.05) from 0
885 in a one sample t-test. The biome abbreviations are: Cropland (CRO), deciduous broadleaf forests
886 (DBF), deciduous needleleaf forests (DNF), temperate evergreen broadleaf forests (EBF-Te),
887 tropical evergreen broadleaf forests (EBF-Tr), evergreen needleleaf forest (ENF), grassland
888 (GRA), mixed forest (MF), savannah (SAV), shrubland (SHR), and wetlands (WET).
889 **Figure 6.** Model predictions of the normalised light-use efficiency responses to soil moisture,
890 expressed as a fraction of the soil moisture saturation point at the top 1 m of soil. The light use
891 efficiency is computed as the ratio between gross primary productivity and the photosynthetic
892 active radiation absorbed by the canopy. The default JULES predictions are in blue and JULES-
893 SOX predictions in red. The lines in the scatter plot panels are linear regressions fit to the data.
894 The histograms on the bottom panels are the soil moisture probability density predicted by each
895 model. The biome abbreviations are: Cropland (CRO), deciduous broadleaf forests (DBF),
896 deciduous needleleaf forests (DNF), temperate evergreen broadleaf forests (EBF-Te), tropical

evergreen broadleaf forests (EBF-Tr), evergreen needleleaf forest (ENF), grassland (GRA), mixed forest (MF), savannah (SAV), shrubland (SHR), and wetlands (WET).

Tables.

Table 1. Residual sum of squares (RSS), number of leaf-level stomatal conductance observations (N) used to fit *n* parameters to the data, and the resulting Akaike Information Criterion differences (ΔAIC) between SOX and the *β*-function.

PFT	N	*SOX*		*β-function*		ΔAIC
		RSS	*n*	RSS	*n*	
BET-Tr	434	4.83	3	6.53	2	-126.1
BET-Te	1334	19.68	3	37.37	2	-853.2
BDT	71	3.48	3	3.04	2	11.6
NET	1571	0.65	3	2.29	2	-1926.4
ESh	133	3.37	3	7.94	2	-112
DSh	64	2.76	3	8.03	2	-66.4

Table 2. Observed (*Obs*) mean (±SD) hydraulic parameters compiled from literature for each plant functional type (PFT) from JULES (Harper *et al.* 2016). The calibrated (*Cal*) columns are the parameter values that maximize JULES-SOX fit to observed GPP in the calibration sites (see Table S2 and Fig. S2).

PFT	Ψ_{50} (MPa)			*a* (unitless)			r_{pmin} (mmol^{-1} m^2 s MPa)		
	N	*Obs*	*Cal*	N	*Obs*	*Cal*	N	*Obs*	*Cal*
BET-Tr	77	-1.9(±1.3)	-1.7	20	4.4(±2.1)	2.1	40	2.2(±3.4)	0.6
BET-Te	44	-2.7(±1.5)	-1.8	17	3.7(±1.8)	2.8	40	3.1(±8)	5

BDT	87	-2.6(±1.4)	-1.6	43	5.5(±3.8)	3.5	31	5.3(±5.6)	0.5
NET	48	-4.2(±1.2)	-2.6	25	8.7(±4.9)	4.9	20	2.4(±1.8)	4.2
NDT	5	-3.4(±0.6)	-1.8	2	7.4(±5)	1.8	2	8(±4.3)	9
C_3	45	-3.1(±1.6)	-2.4	-	-	2.2	-	-	3.2
C_4	15	-2.7(±1.7)	-1.5	-	-	1.8	-	-	9.5
ESh	61	-4(±2.2)	-2.1	53	4.1(±3.3)	2.5	49	1.5(±1.8)	9.5
DSh	26	-4(±2.3)	-1.8	3	3.4(±2.2)	2.1	4	2.6(±2.4)	5

Note: The N column is the number of species compiled for the correspondent parameter.

Table 3. Median Nash-Sutcliffe (1970) model efficiency index (NSE) and root mean square error (RMSE) for the biomes used for evaluating JULES-SOX and default JULES.

Biome	**N**	***JULES-SOX***		***JULES***	
		NSE	**RMSE**	**NSE**	**RMSE**
CRO	3	0.49	123.12	0.57	141.1
DBF	7	0.89	37.32	0.83	47.19
DNF	1	0.58	25.93	0.37	31.97
EBF-Te	3	-0.23	45.22	-1.24	66.36
EBF-Tr	6	0.41	40.36	-2.77	73.53
ENF	5	0.9	34.14	0.59	40.58
GRA	12	0.22	32.31	-0.01	30.62
MF	3	0.85	47.87	0.59	79.29
SAV	5	-0.4	59.72	-2.12	89.69
SHR	4	0.78	14.90	0.64	15.92
WET	21	0.68	32.23	0.46	38.67

Note: The N column is the number of sites representing the biome in the eddy flux dataset

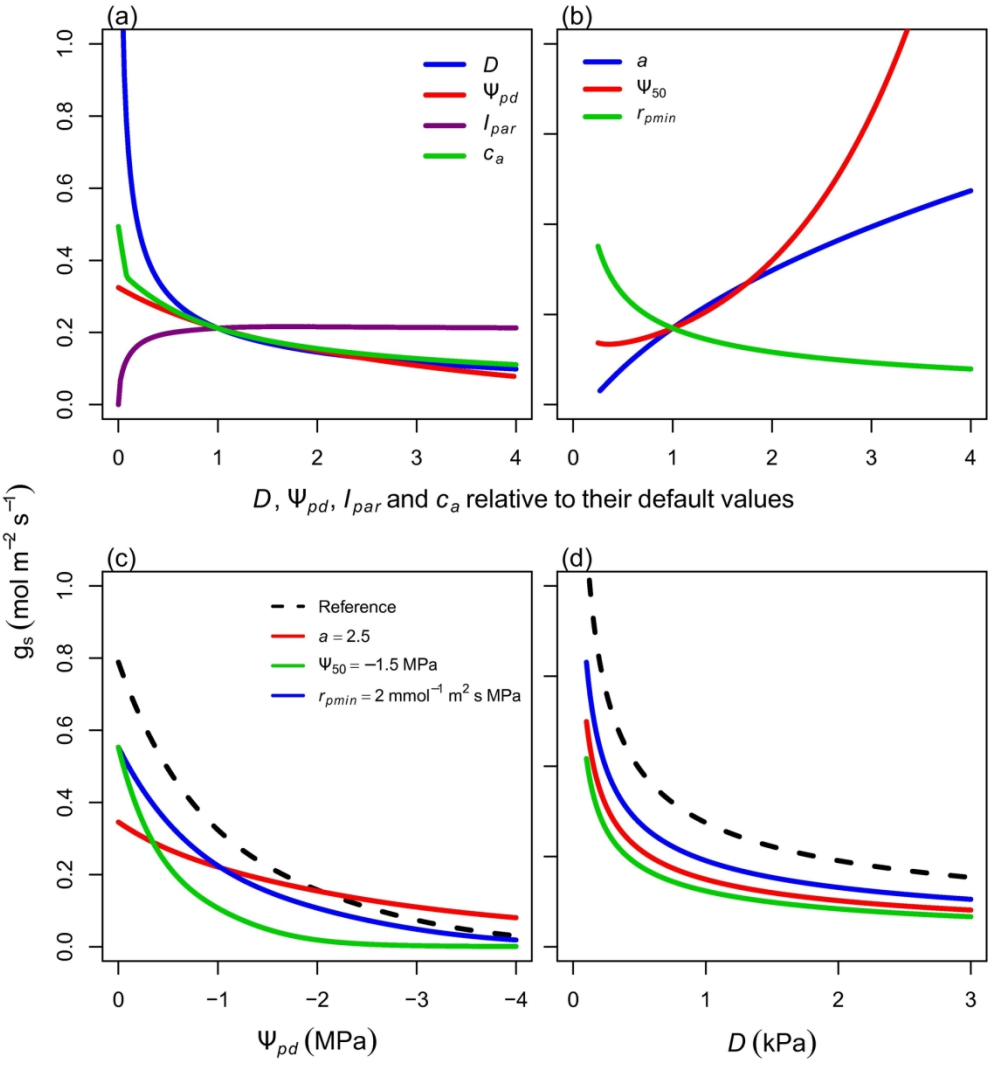

SOX stomatal conductance (gs) sensitivity to environmental drivers in (a) (vapour pressure deficit, D; pre-dawn water potential, Ψpd, Incident photosynthetically active radiation, Ipar, and atmospheric CO2 partial pressure, ca) and plant hydraulic traits in (b) (Ψ when plant loses 50% of its maximum conductance, Ψ50; shape of vulnerability function, a; and minimum plant hydraulic resistance, rpmin). The variables were changed individually while the others were held constant at their reference values (D = 0.5 kPa, Ψpd = -0.5 MPa, Ipar = 600 µmol m-2 s-1, ca = 36 Pa, Ψ50 = -2 MPa, a = 3, rpmin =1 m2 s MPa mmol-1). For the panels (c) and (d) the reference lines (dashed black) represents values of Ψ50 = -3 MPa, a = 5, rpmin =1 mmol-1 m2 s MPa, the coloured lines show how changing each hydraulic parameter affects gs response to Ψpd and D. The Ipar was set to 2000 µmol m-2 s-1 in panels (c) and (d). The Vcmax25 was set to 100 µmol m-2 s and the rest of the photosynthetic parameters follow the BET-Tr parameterization from Harper et al. (2016).

166x188mm (300 x 300 DPI)

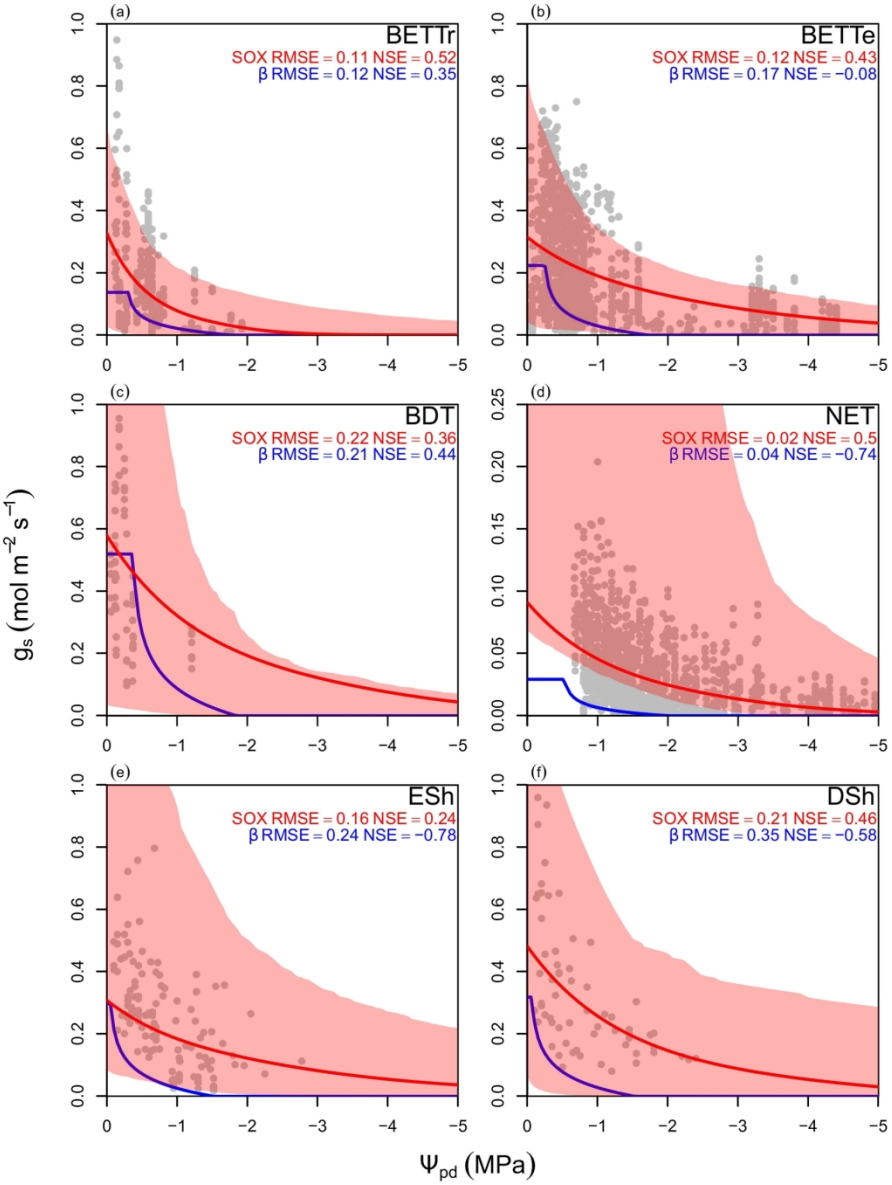

Predicted and observed (grey points) stomatal conductance (gs) response to changes in leaf pre-dawn water potential (Ψpd) for the woody plant functional types (PFT) from Harper et al. (2016), except for Needleleaf deciduous trees which was not present in the dataset used in this study. The red lines are SOX and β-function (Eqn 7-8) best fit. The shaded regions are non-parametric 95% confidence boundaries derived from 1000 bootstrapping replications of the SOX hydraulic inputs. All environmental conditions except Ψpd were held constant at their median values when the gs measurements were taken. The Ψpd was transformed in soil volumetric water content to drive the β-function using Clapp & Hornberger (1978) equations parameterized with soil physical properties derived from the Met Office Central Ancillary Program (Dharssi et al., 2009). The model fit to data is shown as the root mean squared errors (RMSE) and Nash-Sutcliffe (1970) model efficiency index (NSE). The PFT abbreviations are: BET-Tr (Broadleaf evergreen tropical tree), BET-Te (Broadleaf evergreen temperate tree), BDT (Broadleaf deciduous tree), NET (Needleleaf evergreen tree), ESh (Evergreen shrubs) and DSh (Deciduous shrubs).

152x203mm (300 x 300 DPI)

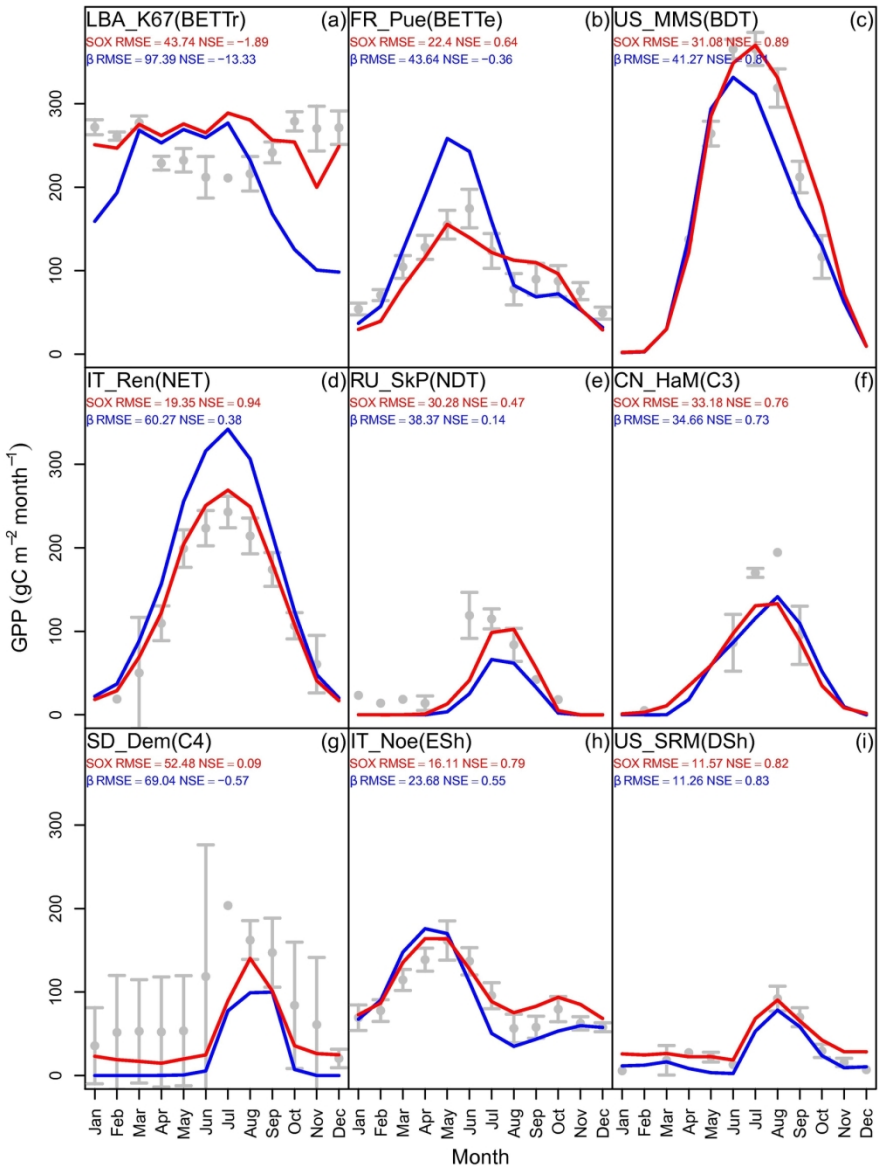

Monthly mean gross primary production (GPP) modelled by default JULES (blue line) and JULES-SOX (red line) versus observations (grey points are means and bars are 2xSE) at each eddy flux site used for calibrating the SOX hydraulic parameters (PFT; Table S2 and Fig. S3). The model fit to data is shown as the root mean squared errors (RMSE) and Nash-Sutcliffe (1970) model efficiency index (NSE). The PFT abbreviations are: BET-Tr (Broadleaf evergreen tropical tree), BET-Te (Broadleaf evergreen temperate tree), BDT (Broadleaf deciduous tree), NET (Needleleaf evergreen tree), NDT (Needleleaf deciduous tree), C3 (C3 grasses), C4 (C4 grasses), ESh (Evergreen shrubs) and DSh (Deciduous shrubs).

152x203mm (300 x 300 DPI)

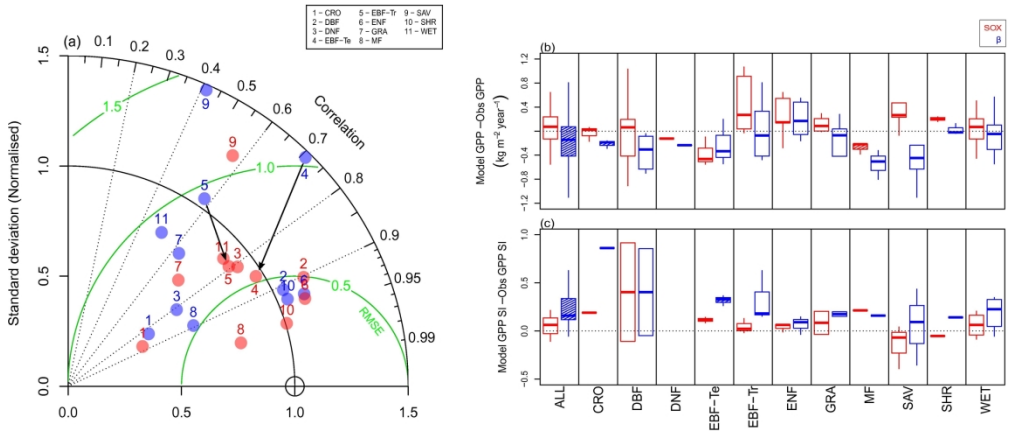

The Taylor diagram (a) shows the difference in JULES and JULES-SOX skill to predict the monthly GPP in each biome. Green lines are the model centered root mean squared errors (RMSE), points closer to the reference circle in the x-axis indicate higher model skill. The two arrows highlight the improvement in model skill for EBF-Tr and EBF-Te. The boxplot panels show the differences between models (default JULES in blue and JULES-SOX in red) and observations in the annual gross primary productivity (GPP in b) and the GPP seasonality (GPP SI in c). Data gaps were excluded from the annual GPP calculations for both models and observations, therefore the differences can be used to evaluate the model skill, but the absolute values do not represent the total annual GPP in each biome. The GPP SI was computed using the approach from Walsh and Lawler (1981). Boxes filled with lines are different (at α=0.05) from 0 in a one sample t-test. The biome abbreviations are: Cropland (CRO), deciduous broadleaf forests (DBF), deciduous needleleaf forests (DNF), temperate evergreen broadleaf forests (EBF-Te), tropical evergreen broadleaf forests (EBF-Tr), evergreen needleleaf forest (ENF), grassland (GRA), mixed forest (MF), savannah (SAV), shrubland (SHR), and wetlands (WET).

218x93mm (300 x 300 DPI)

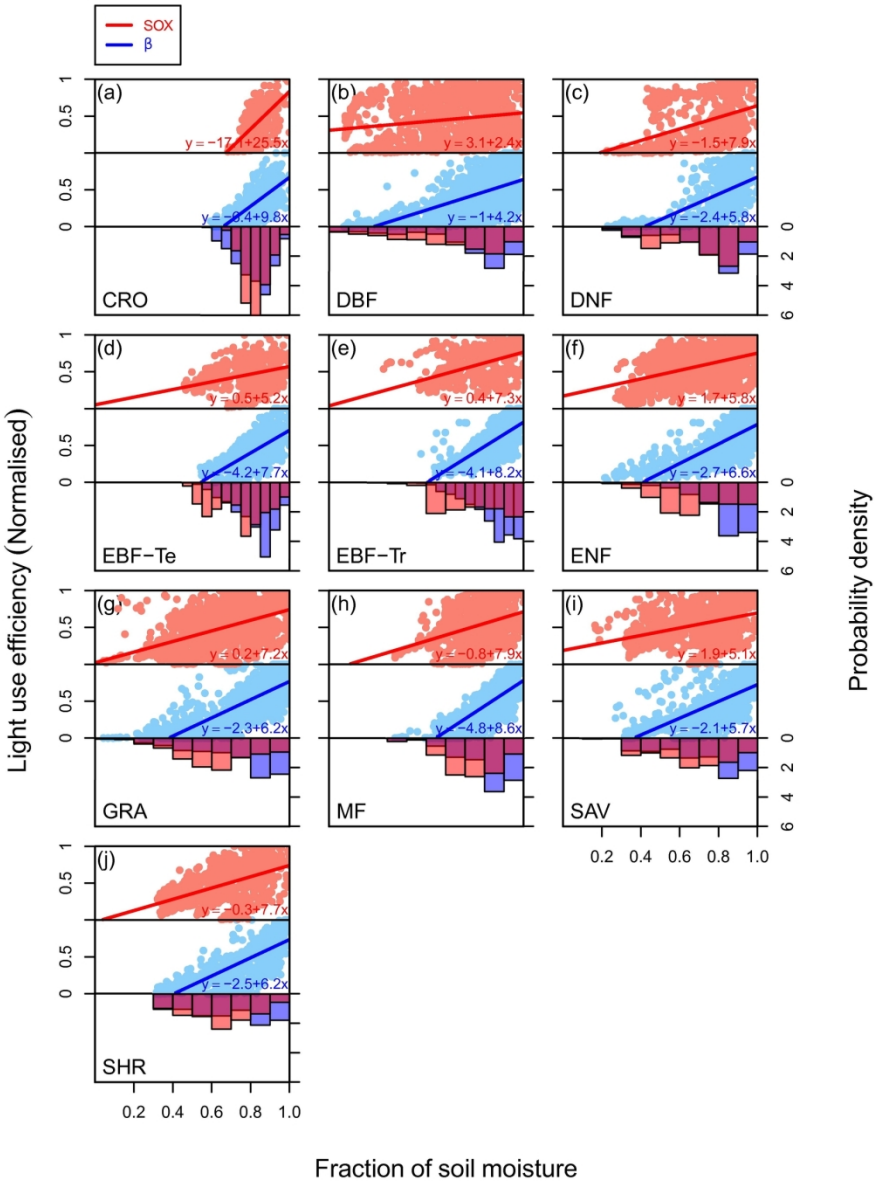

Model predictions of the normalised light-use efficiency responses to soil moisture, expressed as a fraction of the soil moisture saturation point at the top 1 m of soil. The light use efficiency is computed as the ratio between gross primary productivity and the photosynthetic active radiation absorbed by the canopy. The default JULES predictions are in blue and JULES-SOX predictions in red. The lines in the scatter plot panels are linear regressions fit to the data. The histograms on the bottom panels are the soil moisture probability density predicted by each model. The biome abbreviations are: Cropland (CRO), deciduous broadleaf forests (DBF), deciduous needleleaf forests (DNF), temperate evergreen broadleaf forests (EBF-Te), tropical evergreen broadleaf forests (EBF-Tr), evergreen needleleaf forest (ENF), grassland (GRA), mixed forest (MF), savannah (SAV), shrubland (SHR), and wetlands (WET).

152x203mm (300 x 300 DPI)